Int. J. Heat Mass Transfer. Vol. 36, No. 4, pp. 919–924, 1993
Printed in Great Britain

0017-9310/93 $6.00 + 0.00
Pergamon Press Ltd

Modeling of pulsed laser irradiation of thin silicon layers

C. P. GRIGOROPOULOS, H. K. PARK and X. XU
Department of Mechanical Engineering, University of California, Berkeley, CA 94720, U.S.A.

(*Received* 21 *January* 1992 *and in final form* 6 *May* 1992)

Abstract—Interactions of pulsed laser irradiation with matter may lead to controlled phase change transformations and material structure modifications. During transient heating at the nanosecond scale, the thermal gradients across the heat affected zone are accompanied by changes in the material complex refractive index. These changes, coupled with wave interference, modify the energy absorption, and thus the temperature field in the target material. This work accounts for these effects in a rigorous manner using thin film optics theory. Results are presented for the induced temperature field in thin silicon films by pulsed ruby and Nd:YAG laser light.

INTRODUCTION

PULSED laser irradiation is employed over a wide spectrum of materials processing applications, including surface hardening, alloying, curing, synthesis of compound and superconductor films. In semiconductor systems, it is used to anneal ion-implantation surface damage, recrystallize amorphous and polycrystalline films, and enhance dopant diffusion. An extensive review of pulsed laser processing of semiconductors is given in ref. [1].

Both experimental and computational investigations of pulsed laser interactions with semiconductor materials have been performed. A time-of-flight method [2], was combined with time-resolved reflectivity measurements [3] to infer that the energy coupling of pulsed ruby laser light ($\lambda = 0.694$ μm) irradiation of a 20-ns pulse duration with semiconductor materials occurs via a thermal heating mechanism. The measured temperature of the crystal lattice, together with the surface reflectivity of the semiconductor material, clearly indicated melting in accordance with the macroscopic theory of pulsed laser annealing developed by Wood and Giles [4]. The theoretical predictions showed satisfactory agreement with experimental measurements of the melt penetration, melt-duration times, melt-front velocities and dopant concentration profiles in the nanosecond pulsed laser regime at the visible and near infrared wavelengths. Transient conductance measurements [5] yielded the melt depth as a function of time. Numerical heat transfer computations were used to indirectly obtain the transient interface temperature. Nanosecond-resolution, X-ray diffraction measurements [6], of the thermally induced lattice strain yielded temperature profiles in the solid material with an accuracy of ± 50 K. Using time-resolved ellipsometry, Jellison and Lowndes [7] obtained the optical properties of silicon during pulsed excimer laser irradiation.

The transient thermal model of the process [8] agreed with all of the above measurements, with the sole exception of Raman measurements [9, 10]. The optical properties of semiconductors are strong functions of temperature [11]. The treatment of energy absorption in the above mentioned heat transfer models assumes a surface reflectivity that is calculated using bulk expressions and depends upon the surface temperature. The energy absorption is then found by assuming a continuous exponential decay of the radiation intensity in the material. Thin film optics methods [12–14] are used in this work to determine the energy absorption in the target semiconductor material. The effects of a continuously varying complex index of refraction are taken into account. The transient temperature field is calculated via a conductive heat transfer model.

MODELING OF ENERGY ABSORPTION AND HEAT TRANSFER

A sketch of the basic structure is shown in Fig. 1. A silicon layer of thickness d_{si} is deposited on a fused quartz substrate of thickness d_s. The silicon layer is illuminated by a pulsed laser beam. The laser beam diameter on the sample surface is typically 100 μm wide. The temperature profile penetration is of the order of 1 μm. Thus, it may be assumed that the heat transfer at the center of the laser beam is essentially one dimensional. For temperatures below the melting temperature, the conductive heat transfer in the solid silicon layer is given by:

$$(\rho c_p)(T)\frac{\partial T}{\partial t} = \frac{\partial}{\partial x}\left(k(T)\frac{\partial T}{\partial x}\right) + Q_{ab}(x, t). \quad (1)$$

The energy absorption in the semiconductor material depends upon the temperature in the film and is analyzed in the next section. The incident laser intensity considered in this problem is so high (of the order

NOMENCLATURE

a_n	linear coefficient of temperature dependence of the real part of the solid silicon refractive index
c	speed of light
c_p	specific heat
d	layer thickness
d_{si}	semiconductor layer thickness
d_s	substrate thickness
$\mathbf{E}$	electric field vector
F	laser beam fluence
$\mathbf{H}$	magnetic field vector
i	imaginary unit
$\mathbf{i}$	unit vector in the x direction
k	thermal conductivity
k_{ext}	extinction coefficient of silicon
k_{ext}°	extinction coefficient of silicon at 300 K
$\hat{k}$	complex wavenumber
$\mathcal{M}$	transmission matrix
n	real part of the refractive index
n°	real part of the silicon refractive index at 300 K
$\hat{n}$	complex refractive index
N	number of layers in the silicon film
P	temporal profile of the incident laser light intensity
Q_{ab}	energy absorbed by the thin silicon layer, per unit volume, per unit time
R	reflectivity
S	magnitude of the Poynting vector, normalized with the incident energy flux
$\mathbf{S}$	Poynting vector
r	Fresnel reflection coefficient
t	time
t_p	length of laser pulse
t_r	Fresnel transmission coefficient
T	temperature
T_∞	ambient temperature
x	coordinate in the normal to the sample surface direction.

Greek symbols

$\hat{\varepsilon}$	complex electric permittivity
λ	laser light wavelength in vacuum
μ	magnetic permeability
ρ	density
τ	transmissivity
ω	light frequency.

Subscripts

a	ambient
si	silicon
s	substrate.

Superscripts

+	forward wave propagation along the direction of incident laser light
−	reflected wave propagation
*	complex conjugate.

of 10^{12} W m^{-2}), that convection and radiation losses from the top layer surface are negligible. For the time scales considered in this work, the temperature penetration in the structure is small, so that the bottom substrate surface remains at the ambient temperature, T_∞

$$\left.\frac{\partial T}{\partial x}\right|_{x=0} = 0 \tag{2a}$$

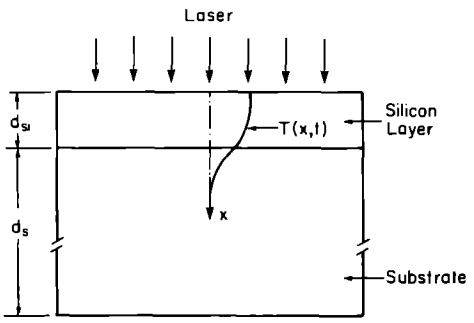

FIG. 1. Sketch of a silicon layer of thickness d_{si}, deposited on a glass substrate of thickness d_s.

$$T(x = d_{si} + d_s, t) = T_\infty. \tag{2b}$$

Initially the structure is isothermal, at the ambient temperature:

$$T(x, 0) = T_\infty. \tag{3}$$

For short times, when the temperature in the silicon layer is below the melting temperature, the heat conduction is solved by an implicit finite difference algorithm.

The temperature field in the semiconductor film induces changes in the material refractive index. The semiconductor film is thus treated as a stratified multilayer structure, composed of N layers of varying complex refractive index (Fig. 2). Assuming that the electric field and the magnetic field are periodic in time, with a time dependence $e^{i\omega t}$, Maxwell's equations for the complex electric and magnetic field vectors become:

$$\nabla \times \mathbf{H} = i\omega\hat{\varepsilon}\mathbf{E} \tag{4a}$$

$$\nabla \times \mathbf{E} = -i\omega\mu\mathbf{H}. \tag{4b}$$

The energy flux along the direction of propagation is

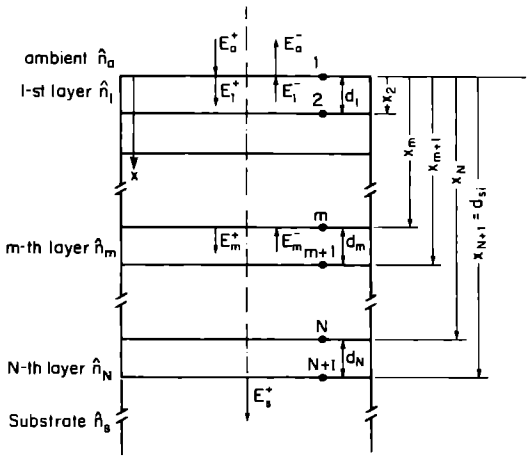

FIG. 2. Schematic picture of the multilayer, stratified structure.

given by the time-averaged magnitude of the Poynting vector:

$$\mathbf{S} = \tfrac{1}{2} Re(\mathbf{E} \times \mathbf{H}^*). \tag{5}$$

A plane wave is incident on the structure, with an electric field amplitude, E_a^+. The corresponding energy flow along the x-direction is:

$$\mathbf{S} = \frac{n_a}{2\mu c} |E_a^+|^2 \mathbf{i}. \tag{6}$$

Utilizing the formalism of the characteristic transmission matrix, the lumped structure reflectivity and transmissivity can be obtained. The mth layer of thickness d_m, which may be absorbing, having a complex refractive index, $\hat{n}_m = n_m - ik_{ext;m}$ is represented by the 2×2 matrix $\mathcal{M}_m$, whose elements are complex:

$$\mathcal{M}_m = \begin{bmatrix} \cos\left(\frac{2\pi}{\lambda}\hat{n}_m d_m\right) & \frac{i}{\hat{n}_m}\sin\left(\frac{2\pi}{\lambda}\hat{n}_m d_m\right) \\ i\hat{n}_m \sin\left(\frac{2\pi}{\lambda}\hat{n}_m d_m\right) & \cos\left(\frac{2\pi}{\lambda}\hat{n}_m d_m\right) \end{bmatrix}. \tag{7}$$

The multilayer transmission matrix, $\mathcal{M}$, is:

$$\mathcal{M} = \prod_{m=1}^{N} \mathcal{M}_m. \tag{8}$$

The reflection and transmission Fresnel coefficients, r and t_r, are:

$$r = \frac{(\mathcal{M}(1,1) + \mathcal{M}(1,2)\hat{n}_s)\hat{n}_a - (\mathcal{M}(2,1) + \mathcal{M}(2,2)\hat{n}_s)}{(\mathcal{M}(1,1) + \mathcal{M}(1,2)\hat{n}_s)\hat{n}_a + (\mathcal{M}(2,1) + \mathcal{M}(2,2)\hat{n}_s)} \tag{9}$$

$$t_r = \frac{2\hat{n}_a}{(\mathcal{M}(1,1) + \mathcal{M}(1,2)\hat{n}_s)\hat{n}_a + (\mathcal{M}(2,1) + \mathcal{M}(2,2)\hat{n}_s)}. \tag{10}$$

The structure reflectivity and transmissivity in terms of r and t_r, follow:

$$R = \frac{|E_a^-|^2}{|E_a^+|^2} = |r|^2 \tag{11}$$

$$\tau = \frac{n_s |E_s^+|^2}{n_a |E_a^+|^2} = \frac{n_s}{n_a} |t_r|^2. \tag{12}$$

The electric field amplitudes of the reflected and transmitted waves, E_a^-, and E_s^+, are obtained using the above expressions. The electric and magnetic fields in the mth layer, $m = 1, \ldots, N$, are given by:

$$E_m(x) = E_m^+ \exp\{-i\hat{k}_m(x - x_m)\} + E_m^- \exp\{+i\hat{k}_m(x - x_m)\} \tag{13}$$

$$H_m(x) = \frac{\hat{n}_m}{c\mu}\{E_m^+ \exp[-i\hat{k}_m(x - x_m)] - E_m^- \exp[+i\hat{k}_m(x - x_m)]\} \tag{14}$$

where

$$\hat{k}_m = \frac{2\pi}{\lambda}\hat{n}_m, \quad x_m = \sum_{l=1}^{m-1} d_l.$$

Continuity of the electric and magnetic field at the interfaces is applied to obtain a recursive formula for the amplitudes of the electric field

$$E_m^+ = \frac{1}{2}\left\{E_{m-1}^+\left[1 + \frac{\hat{n}_{m-1}}{\hat{n}_m}\right]e^{-i\hat{k}_{m-1}d_{m-1}} + E_{m-1}^-\left[1 - \frac{\hat{n}_{m-1}}{\hat{n}_m}\right]e^{+i\hat{k}_{m-1}d_{m-1}}\right\} \tag{15a}$$

$$E_m^- = \frac{1}{2}\left\{E_{m-1}^+\left[1 - \frac{\hat{n}_{m-1}}{\hat{n}_m}\right]e^{-i\hat{k}_{m-1}d_{m-1}} + E_{m-1}^-\left[1 + \frac{\hat{n}_{m-1}}{\hat{n}_m}\right]e^{+i\hat{k}_{m-1}d_{m-1}}\right\}. \tag{15b}$$

Calculation of the amplitudes E_m^+, E_m^-, starts from the first layer, for which $d_{m-1} = 0$. Once the electric field is determined, the power flow is evaluated everywhere in the structure by combining equations (5) and (4). In a location x within the mth layer:

$$\mathbf{S}_m(x) = \frac{1}{2\mu c} Re[(\hat{n}_m)^*(E_m^1(x) + E_m^2(x)) \times (E_m^1(x) - E_m^2(x))^*]\mathbf{i} \tag{16}$$

where

$$E_m^1(x) = E_m^+ \exp[-i\hat{k}_m(x - x_m)] \tag{17a}$$

$$E_m^2(x) = E_m^- \exp[+i\hat{k}_m(x - x_m)]. \tag{17b}$$

The local energy flow is normalized by the energy flux incident on the structure

$$S_m(x) = \frac{1}{n_a|E_a^+|^2} Re[(\hat{n}_m)^*(E_m^1(x)+E_m^2(x)) \times (E_m^1(x)-E_m^2(x))^*]. \quad (18)$$

The absorption in the mth layer is:

$$Q_{ab;m} = P(t)\frac{dS_m}{dx}. \quad (19)$$

RESULTS AND DISCUSSION

A silicon layer of thickness $d_{si} = 0.5$ μm is irradiated by a pulsed ruby laser ($\lambda = 0.694$ μm). The temporal shape of the laser pulse is considered to be equilateral triangular with a pulse length, $t_p = 20$ ns. The laser pulse fluence, F, is defined as the total energy incident on the target during one pulse, per unit target area. Figure 3 shows the surface temperature histories for laser fluences, $F = 0.2$, 0.4 and 0.6 J cm^{-2}. The temperature profiles in the silicon layer for different times, and for a laser fluence, $F = 0.6$ J cm^{-2} are shown in Fig. 4. The absorbed energy as a function of depth for the same times, and laser beam fluence is given in Fig. 5. Initially, and until a time, $t = 8$ ns, the absorption across the silicon layer is periodic with depth. The corresponding temperature profile is relatively flat, as seen in Fig. 4. At longer times, a thermal gradient across the silicon layer is established, and the changes in the material optical properties with temperature

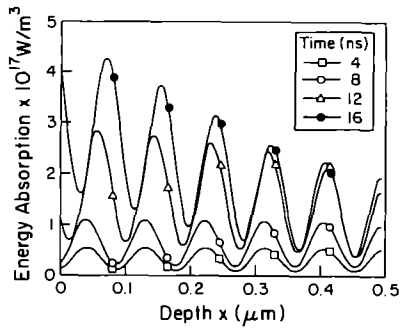

FIG. 5. Absorption profiles in a silicon layer of thickness, $d_{si} = 0.5$ μm, irradiated with a ruby laser. The laser fluence, $F = 0.60$ J cm^{-2}, and pulse length, $t_p = 20$ ns.

(see Appendix) skew the absorbed energy profile towards the irradiated surface, where the temperature (and thus the extinction coefficient, k_{ext}), is larger. The normal reflectivity of the surface for a probing laser wavelength of $\lambda = 0.6328$ μm (HeNe laser) as a function of time, for the laser beam fluences, $F = 0.2$, 0.4, and 0.6 J cm^{-2} is shown in Fig. 6.

The silicon layer is also considered to be irradiated by a frequency doubled pulsed Nd:YAG laser ($\lambda = 0.532$ μm). Silicon is a significantly stronger absorber at this wavelength, and much lower fluences are needed to raise the layer temperature (Figs. 7 and 8). The absorption distribution in the silicon layer (Fig.

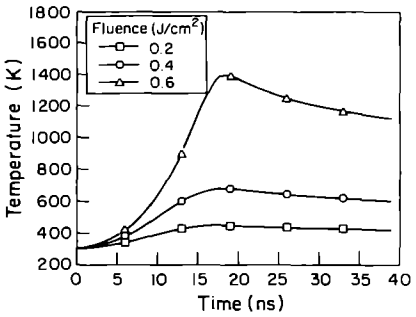

FIG. 3. Surface temperature histories for a silicon layer of thickness, $d_{si} = 0.5$ μm, irradiated with a ruby laser. The laser pulse length, $t_p = 20$ ns.

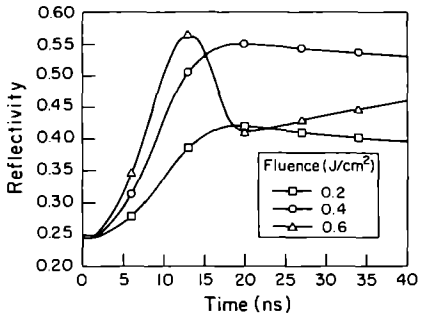

FIG. 6. Normal surface reflectivity histories for a silicon layer of thickness, $d_{si} = 0.5$ μm, irradiated with a ruby laser. The laser pulse length, $t_p = 20$ ns. The probing HeNe laser light wavelength, $\lambda = 0.6328$ μm.

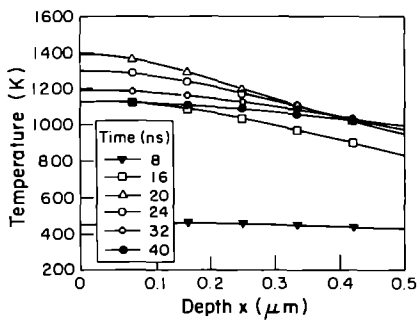

FIG. 4. Temperature profiles in a silicon layer of thickness, $d_{si} = 0.5$ μm, irradiated with a ruby laser. The laser fluence, $F = 0.60$ J cm^{-2}, and pulse length, $t_p = 20$ ns.

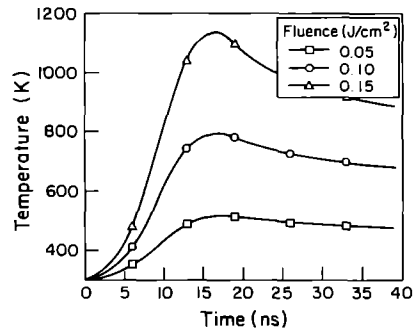

FIG. 7. Surface temperature histories for a silicon layer of thickness, $d_{si} = 0.5$ μm, irradiated with a frequency doubled Nd:YAG laser. The laser pulse length, $t_p = 20$ ns.

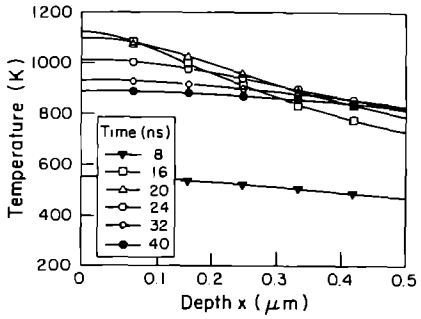

FIG. 8. Temperature profiles in a silicon layer of thickness, $d_{si} = 0.5$ μm, irradiated with a frequency doubled Nd:YAG laser. The laser fluence, $F = 0.15$ J cm^{-2} and pulse length, $t_p = 20$ ns.

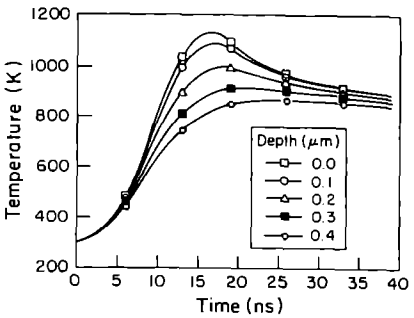

FIG. 11. Transient temperature histories at different locations in a silicon layer of thickness, $d_{si} = 0.5$ μm, irradiated with a frequency doubled Nd:YAG laser. The laser fluence, $F = 0.15$ J cm^{-2}, and pulse length, $t_p = 20$ ns.

9), is consistent with the profiles obtained for the ruby laser case (Fig. 5). The predicted transient reflectivity signals from the irradiated layer surface are shown in Fig. 10. It is seen that the time-resolved surface reflectivity measurements are very sensitive to temperature changes, which should provide valuable information about the silicon layer temperature distribution. The temperature rise at different locations in the silicon layer is shown in Fig. 11. As the distance from the exposed silicon layer surface is increased, the development of the temperature field is progressively, but slightly, delayed.

The above results show that the utilization of thin film optics in a rigorous manner is essential for both the prediction of the temperature distribution in the irradiated semiconductor material, and for the development of optical diagnostic methods at the nanosecond scale. The absorption distribution in the silicon layer exhibits a periodic variation with depth, which is due to wave interference and cannot be captured by the approximating exponential decay assumption. At the nanosecond scale, the temperature field development does not show a corresponding periodic variation within the thin film. Such effects may be observed at shorter time scales. It is noted that the computational approach taken in this work is quite general, and can also be applied to modeling of pulsed laser heating of bulk materials.

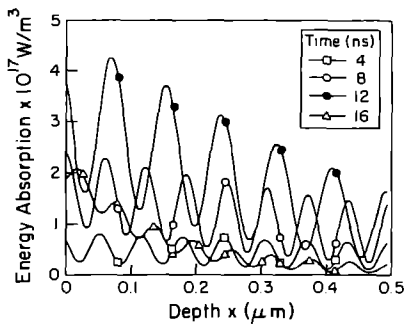

FIG. 9. Absorption profiles in a silicon layer of thickness, $d_{si} = 0.5$ μm, irradiated with a frequency doubled Nd:YAG laser. The laser fluence, $F = 0.15$ J cm^{-2}, and pulse length, $t_p = 20$ ns.

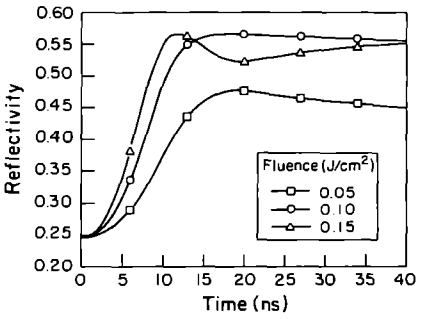

FIG. 10. Normal surface reflectivity histories for a silicon layer of thickness, $d_{si} = 0.5$ μm, irradiated with a frequency doubled Nd:YAG laser. The laser pulse length, $t_p = 20$ ns. The probing HeNe laser light wavelength, $\lambda = 0.6328$ μm.

Acknowledgments—Support for this work by the National Science Foundation, under Grant CTS-9096253, and in part by the Computer Mechanics Laboratory of the University of California at Berkeley, is gratefully acknowledged. The authors benefitted from interaction with Professor Peter Leung of Portland State University, and Dr Andrew C. Tam of the IBM Almaden Research Center, who provided the stimulus for this research.

REFERENCES

1. R. F. Wood, C. W. White and R. T. Young, Pulsed laser processing of semiconductors. In *Semiconductors and Semimetals*, Vol. 23. Academic Press, London (1984).
2. B. Stritzker, A. Pospieszczyk and J. A. Tagle, Measurement of lattice temperature of silicon during laser annealing, *Phys. Rev. Lett.* **47**(5), 356–358 (1981).
3. A. Pospieszczyk, M. A. Harith and B. Stritzker, Pulsed laser annealing of GaAs and Si: combined reflectivity and time-of-flight measurements, *J. Appl. Phys.* **54**(6), 3176–3182 (1983).
4. R. F. Wood and G. E. Giles, Macroscopic theory of pulsed-laser annealing. I. Thermal transport and melting, *Phys. Rev. B* **23**(6), 2923–2942 (1981).
5. R. M. Fastow, J. Gyulai and J. W. Mayer, Transient conductivity measurements in pulsed ion beam melting silicon, *Proc. Materials Research Society* (Edited by J.

Narayan *et al.*), Vol. 13, pp. 69–74. North-Holland, New York (1983).
6. B. C. Larson, C. W. White, T. S. Noggle, J. F. Barhorst and D. M. Mills, Time-resolved study of silicon during pulsed-laser annealing, *Proc. Materials Research Society* (Edited by J. Narayan *et al.*), Vol. 13, pp. 43–50. North-Holland, New York (1983).
7. G. E. Jellison, Jr. and D. H. Lowndes, Time-resolved ellipsometry and reflectivity measurements of the optical properties of silicon during pulsed excimer laser irradiation, *Proc. Materials Research Society* (Edited by D. K. Biegelsen *et al.*), Vol. 35, pp. 113–118. MRS, Pittsburgh (1985).
8. G. E. Jellison, Jr., D. H. Lowndes and R. F. Wood, A detailed examination of time-resolved pulsed Raman temperature measurements of laser annealed silicon, *Proc. Materials Research Society* (Edited by J. Narayan *et al.*), Vol. 13, pp. 35–40. North-Holland, New York (1983).
9. A. Compaan and H. J. Trodahl, Resonance Raman scattering in Si at elevated temperatures, *Phys. Rev. B* **29**, 793–801 (1984).
10. A. Compaan, H. W. Lo, A. Aydinli and M. C. Lee, Pulsed Raman measurements of phonon populations: time reversal, correction factors and all that, *Proc. Materials Research Society* (Edited by J. Narayan *et al.*), Vol. 13, pp. 23–33. North-Holland, New York (1983).
11. G. E. Jellison, Jr. and H. H. Burke, The temperature dependence of the refractive index of silicon at elevated temperatures at several laser wavelengths, *J. Appl. Phys.* **60**(2), 841–843 (1986).
12. R. Jacobsson, Light reflection from films of continuously varying refractive index. In *Progress in Optics* (Edited by E. Wolf), Vol. 5, pp. 247–286. North-Holland, Amsterdam (1965).
13. M. Born and E. Wolf, *Principles of Optics* (6th Edn), pp. 51–70, 611–633. Pergamon Press, Oxford, U.K. (1980).
14. Z. Knittl, *Optics of Thin Films*, pp. 182–282. John Wiley, Prague, Czechoslovakia (1976).
15. Y. S. Touloukian, *Thermophysical Properties of Matter, Thermal Conductivity*. IFI/Plenum, New York (1970).

APPENDIX

Optical properties

In the visible range, the real part of the solid silicon refractive index is a linear function of temperature between approximately 300 and 1000 K [11]

$$n(\lambda, T) = n^{\circ}(\lambda) + a_n(\lambda)(T-300). \quad \text{(A1)}$$

The coefficient $a_n(\lambda)$ is a fifth-order polynomial of the wavelength, λ. The extinction coefficient, k_{ext}, is given by the following expression

$$k_{ext}(\lambda, T) = k^{\circ}_{ext}(\lambda) \exp((T-293)/T_0). \quad \text{(A2)}$$

The complex refractive index components at room temperature for the ruby laser light wavelength ($\lambda = 0.694\ \mu$m) and for the frequency doubled Nd:YAG laser light wavelength, ($\lambda = 0.532\ \mu$m) are given below:

$$n^{\circ}(\lambda = 0.694\ \mu\text{m}) = 3.763 \quad n^{\circ}(\lambda = 0.532\ \mu\text{m}) = 4.153$$

$$k^{\circ}_{ext}(\lambda = 0.694\ \mu\text{m}) = 0.013 \quad k^{\circ}_{ext}(\lambda = 0.532\ \mu\text{m}) = 0.038.$$

In the above expressions, the wavelength, λ, is in μm.

Thermal properties

The solid silicon properties vary with temperature [15]

$$k_{ssi}(T) = 2.99 \times 10^4/(T-99)\ (\text{W m}^{-1}\ \text{K}^{-1}) \quad \text{(A3)}$$

$$\rho_{ssi}(T)c_{p;ssi}(T) = (1.474 + 0.17066 \times T/300) \times 10^6\ (\text{J m}^{-3}\ \text{K}^{-1}). \quad \text{(A4)}$$

The fused silica substrate thermal properties are assumed temperature-independent

$$k_s = 1.4\ \text{W m}^{-1}\ \text{K}^{-2}, \quad \rho_s = 2200\ \text{kg m}^{-3},$$

$$c_{p;s} = 1200\ \text{J kg}^{-1}\ \text{K}^{-1}.$$